Journal of Electroanalytical Chemistry 948 (2023) 117830

Contents lists available at ScienceDirect

Journal of Electroanalytical Chemistry

journal homepage: www.elsevier.com/locate/jelechem

# Oscillations and bistability of complex electrochemical reactions in 3D printed microfluidic devices

John A. Tetteh, Elizabeth A. Hayter, R. Scott Martin, István Z. Kiss *

*Saint Louis University, Department of Chemistry, 3501 Laclede Ave., St. Louis, MO 63103, USA*

A B S T R A C T

We investigate the kinetic features of complex charge transfer chemical reactions using a microelectrode integrated in a flow cell made with 3D printing technology. Thin layer electrochemical cells with 350 μm (height) × 1000 μm (width) channels were designed. Ferrocyanide oxidation on a 100 μm diameter Pt electrode using the printed cell showed mass transfer limiting current at large overpotentials. The variation of the limiting current with the flow rate (1 μL/min ≤ Q ≤ 100 μL/min) was interpreted with the superposition of a constant current due to radial diffusion and a Levich-type square-root relationship, indicating a mixed radial diffusion/thin layer mass transport condition. These findings were further supported by numerical simulation of a diffusion-convection equation in the flow channel. Experiments with copper electrodissolution in phosphoric acid electrolyte reproduced oscillatory behavior that was previously seen in macrocells and polydimethylsiloxane (PDMS) microchips. The 3D printed cell can accommodate multiple electrodes – to demonstrate this application we showed that the current oscillations with copper electrodissolution can exhibit frequency synhcronization with a dual electrode configuration. Finally, hydrogen oxidation on a Pt wire in the presence of $Cu^{2+}$ and $Cl^{-}$ inhibitors displayed bistability at relatively large external resistance and oscillations at high volumetric flow rates. The results show that the 3D printed thin layer design is an alternative to studying nonlinear phenomena in electrochemical cells with distinct advantages to the traditional approaches of using macrocells and PDMS microchip flow cells.

## 1. Introduction

Many electrochemical reactions display complex behavior such as current or potential oscillations and bistability [1]. Mass transport to and from the electrode surface can be used to maintain the reaction at far-from-equilibrium condition, where cell instabilities can occur as a result of fast electrode kinetics, often with positive feedback due to negative differential resistance in the (quasi)stationary voltammetric curves, and the slow negative feedback facilitated by mass transport [2]. Rotating disk electrodes (RDE) have been traditionally used to provide well-defined, reproducible and effective mass transport in electrochemical cells. The effect of rotation rate on complex electrochemical reactions have been extensively studied [3–6]. Commonly, oscillations occur above a minimum rotation rate, because a minimum amount of IR ohmic drop is required and the current increases with the rotation rate according to the Levich equation [6]. In addition, the frequency, the shape, and the region of the oscillations are affected by the rotation rate [7].

One prototype of these complex reactions is metal electrodissolution, for example, copper electrodissolution in phosphoric acid. Current oscillations under potentiostatic conditions can be observed at large overpotentials near the mass transport limited region [4]. The oscillations occur without an external resistance at large [4], or with an attached external resistance with at low rotation rates [5]. Another important class of electrochemical systems that can exhibit complex behavior is electrocatalytic reactions [8]. The electrochemical oxidation of hydrogen in an acidic solution is a well-studied reaction due to its use in $H_2/O_2$ fuel cells [9,10]. Potential oscillations under galvanostatic control have been reported when metal cations and halogen anions are added to the system [11,12]. In previous studies with $Cu^{2+}$ and $Cl^{-}$ using a rotating ring electrode [13], a wide range of dynamical behavior including bistability and oscillations were observed.

Microfluidic cells with integrated electrodes provide an alternative to the RDE setup to investigate electrochemical reactions with well-defined, although rather complex [14], mass transport conditions [15–16]. The electrodes can be made with vapor deposition on a glass substrate for inert electrodes such as Pt [17], or embedded in epoxy for a wide range of electrodes [16]. The flow channels can be made with soft lithography using polydimethylsiloxane (PDMS) [18]. The main dynamical features observed with macroscale RDE system were reproduced with glass-PDMS system with formic acid oxidation on Pt [17], and the epoxy-PDMS system with copper [19] and nickel [20] electrodissolution. It was shown that the large ohmic drops in the flow cells can induce spontaneous oscillations with a single electrode [20] and various

* Corresponding author.
*E-mail address:* istvan.kiss@slu.edu (I.Z. Kiss).

https://doi.org/10.1016/j.jelechem.2023.117830
Received 14 August 2023; Received in revised form 22 September 2023; Accepted 30 September 2023
Available online 2 October 2023
1572-6657/© 2023 Elsevier B.V. All rights reserved.

spatiotemporal patterns including synchronization with electrode arrays [21–24]. One challenging aspect of the soft-lithography based designs include the use of specialized equipment (spin coaters, high intensity UV light source) with many steps (e.g., mask designs) that require optimization in the given laboratory. In addition, the PDMS flow channel can deform at even moderate Reynolds numbers which limits the applications at high flow rates [25].

Numerous gas based reactions such as hydrogen oxidation [13] and carbon monoxide oxidation [26] show complex behavior. However, due permeability of PDMS, the study of gas based reactions in microfluidics proved to be difficult. One attempt supplied the gas directly to the working electrode [27]. However, diffusion of the gas through the PDMS membrane still remained a problem with as much as 30 % of the gas diffusing in 5–10 min. Another method used encased the cell in a plexiglass box with constant gas flow in and out of the [28].

The use of 3D printing as an alternative to glass and PDMS for creating microfluidic devices is a rapidly developing research area. [29–30] Electrochemical detection in a 3D-printed fluidic system used a threaded device where electrodes fabricated in commercially available polyetheretherketone (PEEK), fittings could be integrated as desired. [31] The thin-layer design provided flexibility of electrode materials for amperometric deteciton of dopamine as well as ease of electrode replacement after fouling or electrode polishing. Subsequent work included use of 3D printing to create devices with a wall-jet configuration, [32] robust microfluidic devices that integrate with electrochemical biosensors for detecting glutamate, glucose and lactate in microdialysates, [33] and multimodal devices that can be used to detect both ATP (via chemiluminscence) and nitric oxide (via amperometry) release from red blood cells. [34].

In this paper, we explore kinetic features of complex electrochemical reactions in a 3D printed microfluidic flow cell. 3D printing is used for the construction of a cell with electrodes, either a platinum or copper electrode, integrated into the flow channel. The relationship between flow rate and limiting current is determined using ferrocyanide oxidation. The observed mass transport limited behavior is compared to a simulation of the concentration profile in the flow channel with diffusion-convection equations. The dynamical behavior of copper electrodissolution in phosphoric acid is studied with both single and dual working electrode configurations and compared to previous studies in a PDMS microfluidic cell. The feasibility of achieving hydrogen oxidation in the 3D printed cell is tested as well as the effect of external resistance and flow rates on the occurrence of bistability and oscillations. The potential of the applications of 3D printed cells for studying nonlinear dynamics of complex electrochemical systems is discussed.

## 2. Material and methods

### 2.1. Chip and electrode fabrication

The 3D printed device with a 350 μm (width) × 1000 μm (height) channel was designed using Autodesk Inventor Professional 2014 and printed using a Stratasys J750 PolyJet printer with Vero UltraClear model material and associated support material. The channel dimensions were confirmed with optical measurements resulting in 352 μm × 1004 μm channel. A schematic representation of the 3D printed device including the placement of the working, reference, and counter electrode as well as the flow of the solution in the chip are shown in Fig. 1a and b. Details about the construction of the chip are provided in

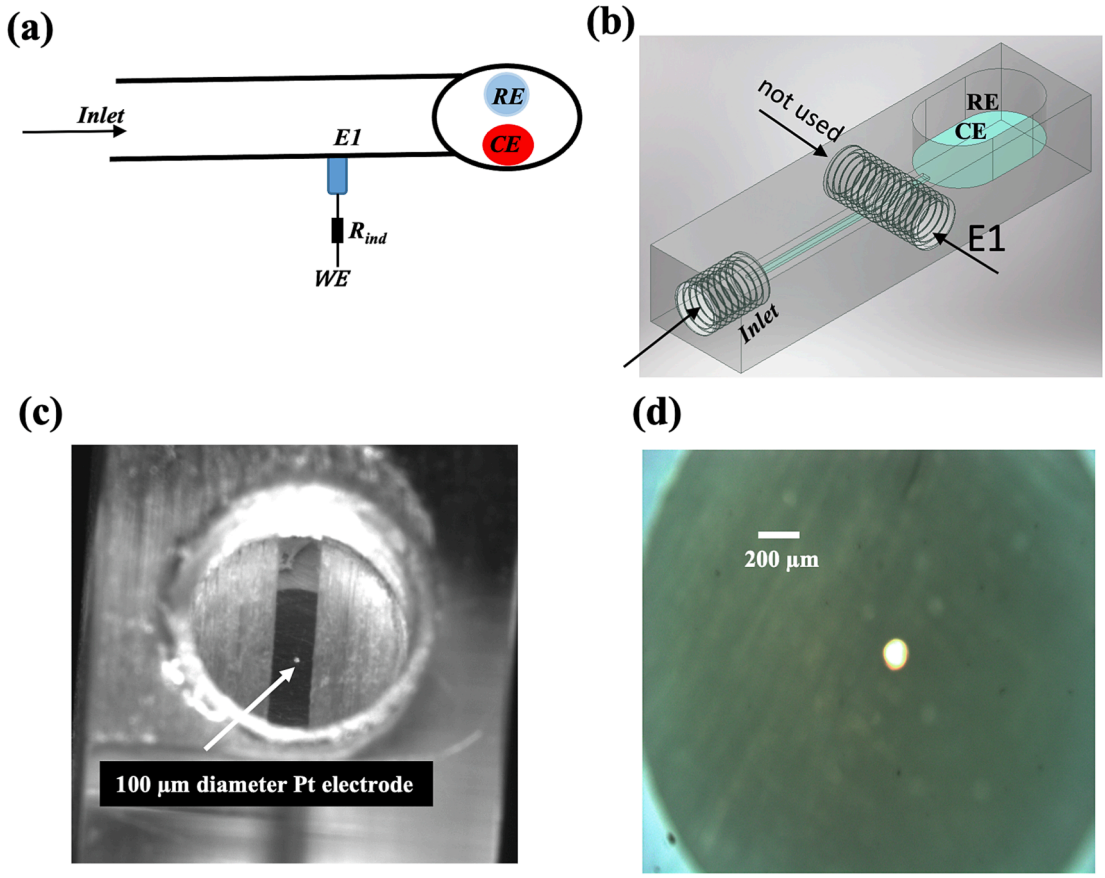


**Fig. 1.** Experimental design. a) A schematic representation of the 3D printed electrochemical cell including inlet, 100 μm diameter platinum or 80 μm diameter copper working electrode (WE), 0.5 mm diameter platinum counter electrode (CE), and a Ag/AgCl/3M NaCl reference electrode (RE). b) The designed 3D printed cell. c) Optical microscope image of a 100 μm diameter platinum working electrode in direct contact with the flow channel of the 3D printed device. d) Optical microscope image of the surface of the working electrode, showing the 100 μm diameter platinum wire embedded in epoxy within the PEEK nut.

previous work [35]. Working electrodes (100 μm diameter platinum wire or 80 μm diameter copper wire) were set in epoxy (Armstrong C7 with activator A, Ellsworth Adhesives) within a PEEK fitting nut (5/16-24-1/8LT, IDEX Health & Science). With copper electrodissolution when two working electrodes were used, the two electrodes were placed at a distance of 8 mm in two configurations, close and far placements, where the distance from the downstream electrode to the reservoir was 8 mm and 16 mm, respectively. The flow channel and the surface of the working electrode are shown in Fig. 1c and d.

### 2.2. Electrochemical experiments

The working electrode, housed within the PEEK fitting, was first polished in order to ensure that a clean surface of the metal was exposed. The copper electrode was polished with grit paper (P1200 and P4000) and a grinder-polisher (Buelher Metaserv 3000). Platinum was wet polished using 0.05 μm alumina. The working electrode was wrapped in Teflon tape to ensure a tight fit when screwed into the 3D printed device. These electrodes can be repolished and reused as desired. The device was designed so that the WE was directly in contact with the electrolyte flow (see Fig. 1c). A Ag/AgCl/3M NaCl reference electrode and a 0.5 mm diameter titanium rod coated in platinum counter electrode were placed in the reservoir. The flow of solution was established using a Harvard Apparatus pump. A SGE syringe was connected to the WTE via Tygon tubing and a Finger Tight I Peek fitting (IDEX). Polarization scans were performed using a Gamry Reference 600 potentiostat at room temperature. Data was acquired at a rate of 1 kHz.

Three experiments with varying experimental conditions were performed with ferrocyanide oxidation, copper electrodissolution, and hydrogen oxidation. With ferrocyanide oxidation, a solution of 1 M potassium nitrate (99+%, ACROS Organics), 0.01 M potassium *hexa*-cyanoferrate (II) (Sigma Aldrich)/0.02 M potassium ferrocyanide (ACROS Organics) was made using milipore water and purged with nitrogen gas 45–60 min prior to experiment. For copper electrodissolution, 85 % o-phosphoric acid was pumped through the device at a flow rate of 100 μL/min. Linear polarization sweeps were performed at 5 mV/s. With hydrogen oxidation, hydrogen gas was bubbled through a solution of sulfuric acid, copper (II) sulfate pentahydrate (ACROS Organics), and hydrochloric acid 1 h prior to experiment. Two different solutions were used which varied in the concentrations of the components. The first solution contained 0.5 M $H_2SO_4$, $5x10^{-5}$ M $CuSO_4$, and 0.1 M HCl. The second solution was made of $0.5x10^{-3}$ M $H_2SO_4$, $10^{-5}$ M $CuSO_4$, and $10^{-4}$ M HCl.

## 3. Results and discussion

To confirm the experimental design of the 3D printed reactor, first ferrocyanide oxidation was studied at various flow rates in the 3D printed flow cell to establish the relationship between current and volumetric flow rate. The behavior of copper electrodissolution was studied in the 3D printed device and compared to that observed in a PDMS flow cell. Finally, hydrogen oxidation in the presence of copper (II) and chloride ions was performed in the 3D printed device.

### 3.1. Ferrocyanide oxidation

Linear sweep voltammetry (LSV) was performed at various flow rates ($Q$) during ferrocyanide oxidation. Fig. 2a shows the LSV

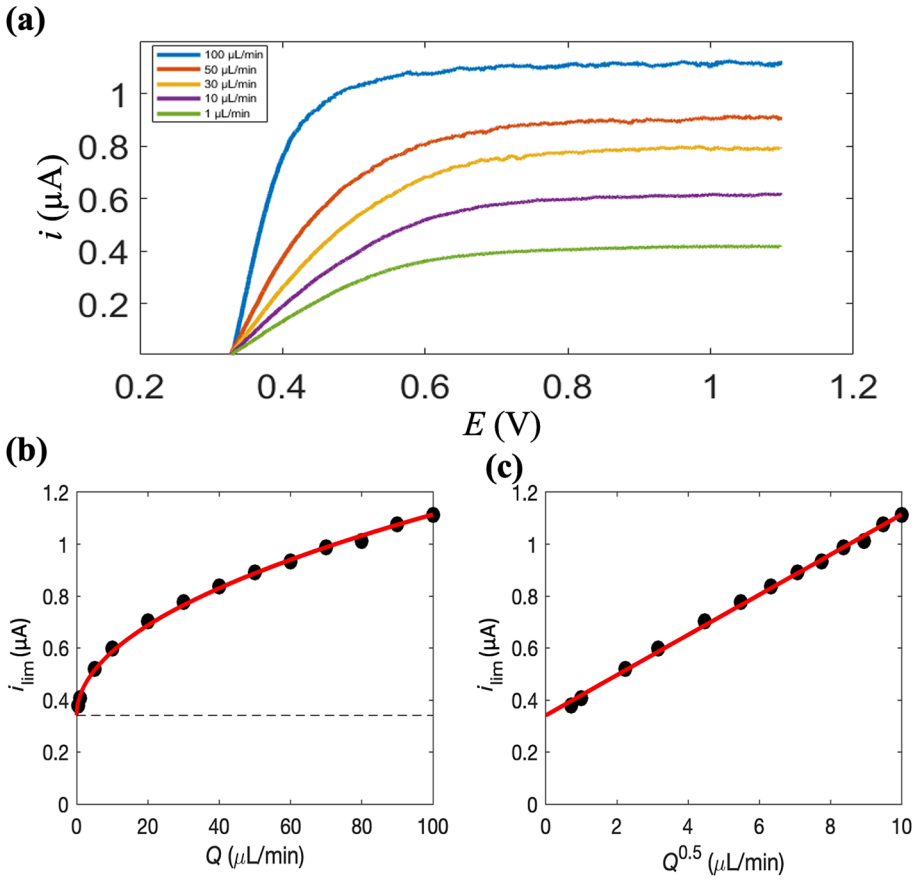


**Fig. 2.** Voltammetric curves and dependence of limiting current on flow rate with ferrocyanide oxidation on platinum in the 3D printed cell. a) Linear seep voltammograms at different flow rates showing limiting current at large circuit potentials. b) Limiting current as a function of flow rate (circles) and a modified Levich fit (curve) using Eq. (1). c) Limiting current as a function of the square root of the flow rate (circles) and a least square fit (line).

voltammograms with flow rates of 1–100 μL/min. Each scan showed a limiting current ($i_{lim}$). As the flow rate increased, the limiting current increased from 0.40 μA to 1.11 μA indicating that the reaction is mass transfer controlled. The limiting currents and their corresponding flow rates are shown in Fig. 2b. The limiting current increases with flow rate nonlinearly. The variation can be interpreted with the superposition of a constant term (α) with a Levich-type square-root dependence [36] on $Q$:

$$i_{lim} = \alpha + \beta Q^{0.5} \quad (1)$$

where β is fitting factor. Fig. 2c shows that a (nearly) linear relationship can be obtained when $i_{lim}$ is plotted vs. $Q^{0.5}$, and the obtained fitting coefficients ($\alpha = 3.41 \times 10^{-1}$ μA and $\beta = 7.73 \times 10^{-2}$ μA min$^{0.5}$ μL$^{-0.5}$) can reproduce well the experimental data (line in Fig. 2b).

The validity of Eq. (1) implies that the mass transport conditions in the 3D printed device are in a mixed region where both constant current, likely due to radial diffusion, and thin-layer conditions with Levich-type dependence should be considered. To confirm this hypothesis, we performed numerical simulations with a 2D model of dimensionless diffusion-convection equations [14],

$$\frac{\partial C}{\partial \tau} = \frac{\partial^2 C}{\partial X^2} + \frac{\partial^2 C}{\partial Y^2} - V_X(Y)\frac{\partial C}{\partial X} \quad (2)$$

where $X = x/h$ and $Y = y/h$ are the dimensionless length and height of the channel, $h$ is the channel height, $C = c/c_0$ is the dimensionless concentration, $c_0$ is the concentration of redox species, $\tau = Dt/h^2$ is the dimensionless time, $D$ is the diffusion coefficient, $V_X(Y) = 6\mathrm{Pe}Y(1-Y)$ is the flow velocity, $\mathrm{Pe} = u_{av}h/D$ is the Peclet number, and $u_{av}$ is the mean flow velocity. The boundary conditions are $C = 1$ at the microchannel entrance (inlet), $C = 0$ (corresponding to fast charge transfer kinetics that consumes the analyte completely and thus the rate is controlled by mass transport) at the electrode surface (positioned at $Y = 0$ and $X = 1$ to $1 + W$, where $W = w/h$ is the dimensionless electrode width, $w$ is the electrode width), and no-flux otherwise. The steady state solutions ($\partial C/\partial \tau = 0$) were obtained with COMSOL Multiphysics finite element simulations software, and the dimensionless current, $\Psi = i/(NFLDc_0) = \int_0^W |\partial C/\partial Y|_{Y=0}$ are shown as a function of Pe in Fig. 3a. In the experimentally relevant region (1 μL/min ≤ Q ≤ 100 μL/min) with Peclet numbers about 1 to 2500, Ψ increases nonlinearly with Pe. Similar to the experiments, very good fit to the data can be obtained by superimposing a constant value (0.161) to a Levich-like ($\mathrm{Pe}^{0.5}$) contribution as shown in Fig. 3 a and b. The concentration profiles indicate that as Pe is increased, the nearly radial diffusion behavior (Fig. 3c, Pe = 10) transforms to a mixed (Fig. 3d, Pe = 100) and then a thin-layer (Fig. 3e, Pe = 1000) type. It should be emphasized that the simulations in Fig. 3 do not include many additional factors, e.g., potential drops in the electrolyte with ion migrations and the variation of concentration profiles in the 3rd dimension, i.e., the depth of the channel.

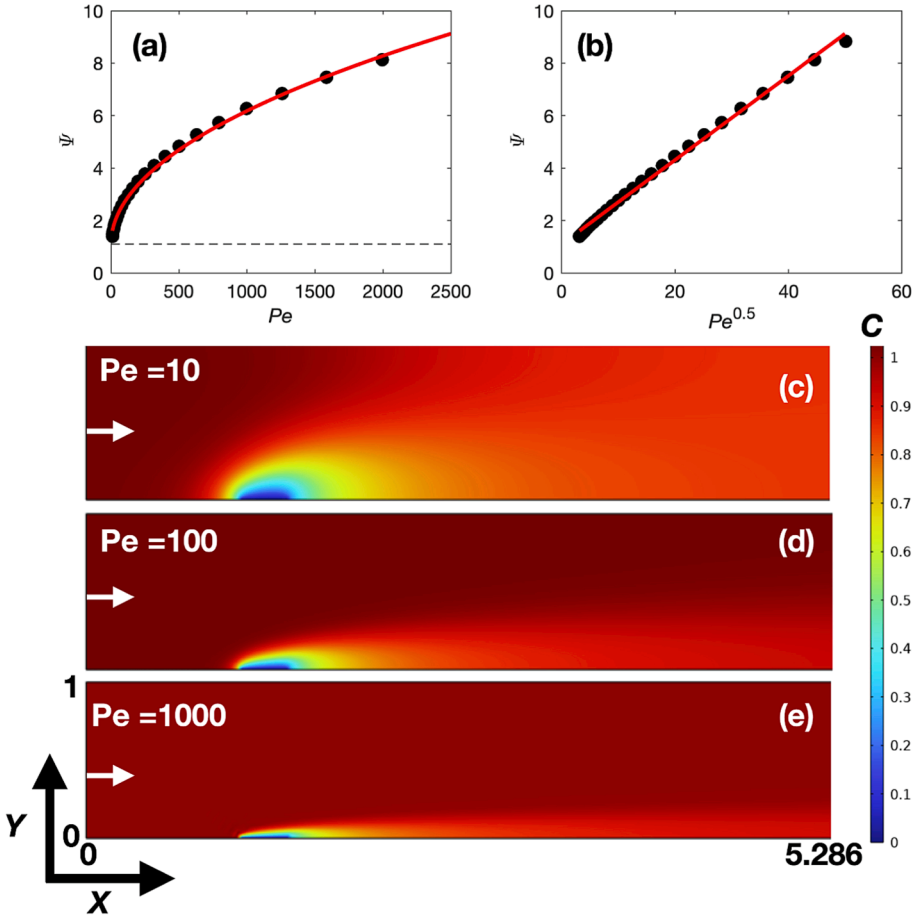


**Fig. 3.** Simulation of diffusion-convection equation in a rectangular microchannel. a) Dimensionless limiting current, Ψ, as a function of Peclet number, Pe, (circles) and a modified Levich fit (curve) using Eq. (1) with Ψ in Pe in place of $i_{lim}$ and Q, respectively. b) Ψ as a function of square root of Pe (circles) and a least square fit (line). c-e) Concentration profile ($C$) for Pe = 10, 100, and 1000. A 5.286 (width) × 1 (height) dimensionless unit rectangle was considered with an electrode with $W$ = 0.286 (100 μm electrode width divided by 350 μm channel height) located at $X$ = 1 to 1.286 and $Y$ = 0. Boundary conditions: $C$ = 1 for inlet (denoted as arrows), $C$ = 0 for the electrode, and no flux otherwise. The bottom left corner is at $X = Y = 0$.

Nonetheless, the simulations do confirm the experimental findings and clarify the observed nonlinear dependence of the limiting current on the flow rate.

We thus see that the 3D printed electrochemical cell facilitates effective mass transport with well-characterized scaling. To search of oscillatory behaviors, we focused on high flow rates (e.g., Q ≈ 100 μL/min and above), which represent thin-layer/Levich type scaling similar to those observed with the corresponding RDE studies with copper electrodissolution [5] and hydrogen oxidation reactions [13].

### 3.2. Copper electrodissolution

Copper electrodissolution in phosphoric acid was studied using the 3D printed cell with a 80 μm diameter copper electrode. Repeated LSV voltammograms were performed in the system at a flow rate of 100 μL/min (scan rate = 5 mV/s, see Fig. 4a). With increasing the electrode potential, the current first increases, then exhibits a peak with a decreasing current (negative different resistance) and a limiting current at large potentials. The limiting current decreased with each successive scan. The limiting current was 3.80 μA, 2.92 μA, 2.33 μA, 1.95 μA, and 1.74 μA for scans 1,2,3,6, and 7 respectively. The largest decrease of 0.88 μA was between scans 1 and 2, and the decreased lessened as the number of scans increased.

Copper electrodissolution was previously studied in a PDMS flow cell but a significant amount of drift was observed in the limiting current after linear polarization scans [37]. During repetitive linear polarization scans in the PDMS flow cell, the limiting current decreased by 64 % during seven scans with the largest decrease occurring between scans two and three. With 3D printed flow cell, this drift (which can be attributed to the recessing copper electrode and the corresponding less intense mass transport condition) is less, as the polarization scans in the 3D printed flow cell showed a decrease in limiting current by 54 % over seven scans with the largest decrease occurring between scans one and two. Nonetheless, the behavior of the copper electrodissolution in the 3D printed flow cell is comparable to those seen in a PDMS flow cell. [37].

External resistance was added to the 3D printed cell ($R$ = 250 kΩ) and current oscillations were observed for 1.05 V < $E$ < 1.19 V (see Fig. 4b). Note that as expected, the current oscillation occur on the negative slope of the i/E curve because in the copper electrodissolution system the oscillation can be interpreted with $N$-shaped negative differential resistance ($N$-NDR) polarization curve. [5] Current oscillations at constant potential ($E$ = 1120 mV) with external resistance ($R$ = 250 kΩ) are shown in Fig. 4c. The oscillations occurred at a frequency of 1.07 Hz and amplitude of 0.53 μA. In comparison, smooth current oscillations with a frequency of 2.07 Hz and amplitude of 0.50 μA were observed in the PDMS cell with a somewhat larger electrode (100 μm diameter) and correspondingly smaller external resistance $R_{ext}$ = 100 kΩ [19]. (Note that the required resistance for the oscillations depends on the electrode surface area. [6]) All together, the experiments showed that the 3D printed flow cell can be used as an alternative to the PDMS based cell for studying current oscillations with copper electrodissolution.

The 3D printed cell can be equipped with multiple working electrodes. With oscillatory reactions, the metal dissolution can take place with or without synchronization. Fig. 5 shows the results in a 3D printed cell with two copper wires. When the two wires were placed 8 mm apart and the downstream electrode was placed at a distance of 8 mm to the reservoir, the current oscillations are not synchronized (see Fig. 5a) because they have different frequencies (0.982 Hz and 1.116 Hz). In contrast, when the electrodes with the same distance were placed further away from the reservoir at a distance of 16 mm, the oscillations are synchronized because the frequencies are the same, 0.978 Hz (see Fig. 5b). These experiments thus demonstrate that the cell design plays an important role in the behavior of the current oscillations; similar studies in the past were performed with nickel electrodissolution under kinetic control where standing electrodes can be used [22]. The 3D printed technique will enable investigations of synchronization of current oscillations with multielectrode arrays for a wide range systems that require mass-transport control to keep the system sufficiently far from equilibrium for the oscillations to occur.

### 3.3. Hydrogen oxidation

Hydrogen oxidation using a 100 μm platinum electrode in the 3D system was studied. A cyclic sweep voltammogram was performed when no hydrogen gas was added to the cell (Fig. 6a). As expected, the currents are small (<10nA before water electrolysis at high overpotentials) with a small anodic and cathodic peaks due to the formation of platinum oxides.

Hydrogen gas was added to the cell with no resistance attached to the electrode (see Fig. 6b). In the forward scan, the current starts to increase at $E$ = 0.40 V due to hydrogen being oxidized. The current reaches a maximum of $i_p$ = 60nA at $E$ = 0.56 V and then the current begins to decrease (negative differential resistance) as the chloride ions adsorb on the electrode surface. At even higher potentials of 1.20 V, the current increases due to water electrolysis. Both the forward and backward

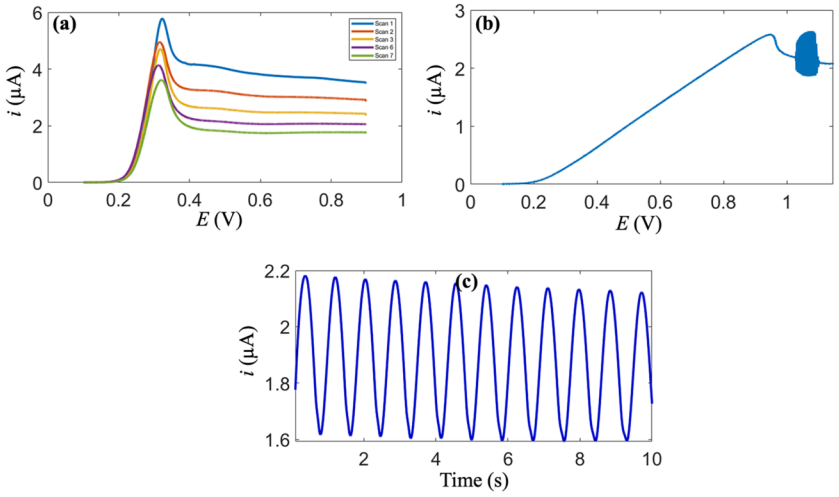


**Fig. 4.** Copper electrodissolution in concentrated phosphoric acid. a) Repeated linear sweep voltammograms of copper electrodissolution. Consecutive scans were performed by scanning the potential forward. Scan rate = 5 mV/s. b) Current oscillations during linear sweep with external resistance (R = 250 kΩ). Scan rate = 5 mV/s. c) Current oscillations at constant potential ($E$ = 1120 mV) with external resistance ($R$ = 250 kΩ). Q = 100 μL/min.

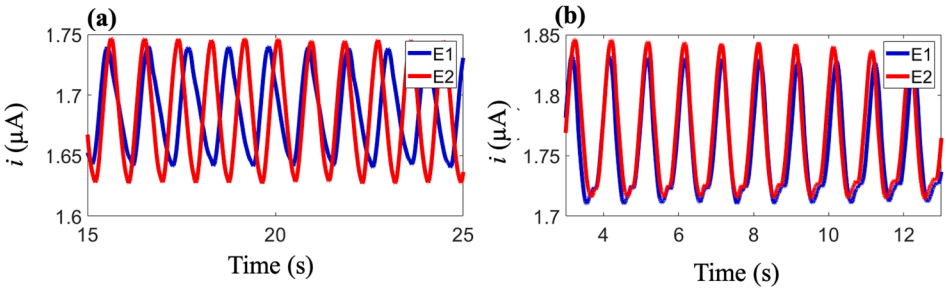


**Fig. 5.** Synchronization patterns with a dual working electrode setup with copper a) Desynchronized current oscillations with close placement ($L$ = 8 mm) to the reservoir. b) Synchronized current oscillations with far placement (L = 16 mm) to the reservoir. $R$ = 250 kΩ, $E$ = 1180 mV, $Q$ = 100 μL/min.

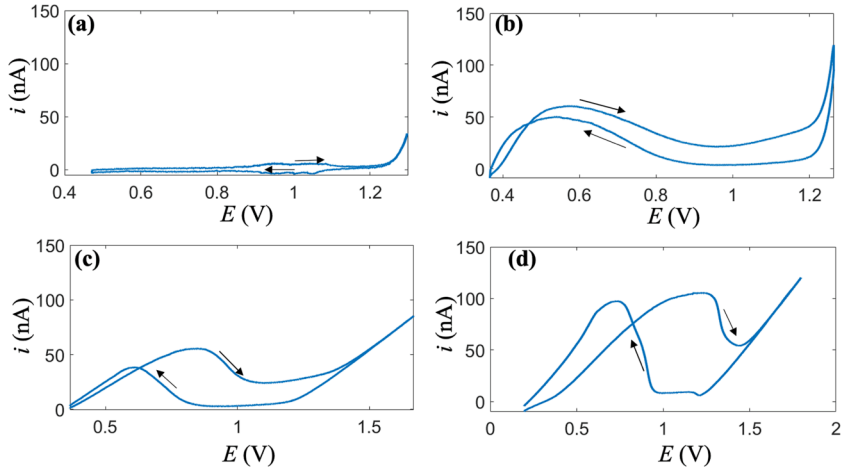


**Fig. 6.** Emergence of bistability with added external resistance shown in polarization curves of hydrogen oxidation using 0.1 M HCl, 5x10$^{-5}$ M, $CuSO_4$, and 0.5 M $H_2SO_4$ electrolyte with a 100 μm diameter platinum wire. a) No hydrogen gas added to solution. b-d) Hydrogen gas added, with varying external resistance ($R$). b) $R$ = 0 Ω. c) $R$ = 6 MΩ. d) $R$ = 16 MΩ. $Q$ = 100 μL/min, scan rate = 10 mV/s.

scans are similar with a small change (drift) that can be related to changes in surface conditions. Bistability begins to emerge when external resistance ($R$ = 6 MΩ) is added (Fig. 6c). In this bistable region, during the forward scan the current starts to decrease at $E$ = 0.88 V (with current value of 54nA), but in the reverse scan the current starts to increase from a low value of 4.2nA at $V$ = 0.83 V. We thus see that there is a bistability for 0.83 V < E < 0.88 V; in this region the current is large (>50nA) during the forward, and low (<10nA) during the backward scan. Note that these changes are not due to the small change in surface conditions (as in Fig. 6b) because at low ($E$ <0.60 V) and high ($E$ >1.42 V) circuit potentials the currents are similar in both directions. As expected, when an even larger resistance is added ($R$ = 16 MΩ), the bistable region increases (0.95 V < $E$ < 1.48 V) as shown in Fig. 6d.

To further investigate the dynamics, the concentrations of the electrolytes in solution were decreased to 1x10$^{-4}$ M HCl, 1x10$^{-5}$ M, $CuSO_4$, and 0.5x10$^{-3}$ M $H_2SO_4$. With external resistance ($R$ = 30 MΩ) and a flow

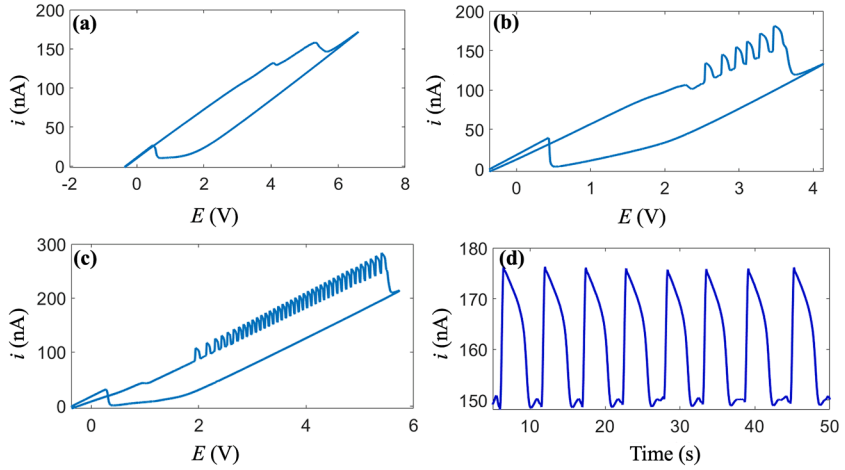


**Fig. 7.** Effect of flow rate on occurrence of bistability and oscillations in polarization curves of hydrogen oxidation in the presence in 1x10$^{-4}$ M HCl, 5x10$^{-5}$ M, $CuSO_4$, and 0.5x10$^{-3}$ M $H_2SO_4$ electrolyte using a 100 μm diameter platinum wire. Scan Rate = 10 mV/s and $R$ = 30 MΩ. a) $Q$ = 100 μL/min. b) $Q$ = 200 μL/min. c) $Q$ = 350 μL/min. d) Current oscillations at constant potential ($E$ = 3200 mV) and $Q$ = 350 μL/min.

rate of 100 μL/min, the system displays bistability in a large range of 0.08 V < $E$ < 5.80 V (Fig. 7a). When the flow rate is increased to 200 μL/min, the system exhibits oscillations during the forward scan (Fig. 7b). However, these oscillations are relatively weak and disappear quickly at $E$ = 3.80 V. The flow rate was then increased further to 350 μL/min as shown in Fig. 7c. The bistability occurs in a large circuit potential range 0.05 V < $E$ < 5.80 V. The oscillations are now robust and exist over a large potential range (2.00 V < $E$ < 5.80 V). The current oscillations are shown in Fig. 7d at constant circuit potential (E = 3200 mV); the oscillation has a frequency of 0.18 Hz and amplitude of approximately 26.4nA. Note that with hydrogen oxidation, the current oscillations occur on the positive slope of the i/E curve, in contrast with copper electrodissolution, where the oscillations occurred on the negative slope. This is because the mechanism of the current oscillation with hydrogen oxidation can be interpreted with a hidden negative differential resistance (HN-NDR), [8] where the negative differential resistance (due to $Cl^-$ adsorption) is hidden due to a slow activation of the catalytic surface (due to the desorption of the $Cu^{2+}$ ions).

Hydrogen oxidation in the presence of copper (II) and chloride ions in macrocell was previously studied and dynamical behavior was characterized [12–13,38–39]). Similar behavior was observed here with the 3D printed device, which is made of a hard, acrylate-based plastic (VeroClear) that is not gas permeable. Bistability occurred when a minimum amount of resistance was added to the cell. Previous rotating ring experiments showed hydrogen oxidation to have hidden negative differential resistance (HNDR), which allows for oscillations to occur [13]. HNDR (i.e., NDR hidden by a slow positive differential resistance process) was also observed in the 3D printed cell and oscillations occurred on the positive slope of the forward potential scan. These current oscillations occurred at lower electrolyte concentrations. For comparison, we also attempted to study hydrogen oxidation with PDMS-based flow cells in the previous setup; [19] however, without a sealed plexiglass box covering the flow cell, the $H_2$ diffused very quickly out of the gas permable PDMS-based flow channel, and reproducible results showing bistability and oscillations were not obtained. These results thus show that the 3D printed device can be used effectively to investigate the nonlinear dynamics of $H_2$ electro-oxidation, without the need for external mechanisms to limit diffusion of $H_2$ from the device (as is the case when using PDMS devices).

## 4. Conclusions

We have shown that a 3D printed flow cell can be used to investigate complex chemical reactions. Mass transport can be effectively tuned with the flow rate: the limiting current has a Levich-like dependence on flow rate with a scaling power of about 0.5 above a constant value. For the typical flow rates applied here (1 μL/min ≤ $Q$ ≤ 100 μL/min) with Peclet numbers (1≤ Pe ≤2500) we see a transition from mixed radial diffusion/thin layer mass transport condition to a classical thin layer/Levich region, corresponding to a transition between regions IVb and III according to the proposed classification scheme for microband electrodes in flow channels. [14]) The 3D printed device provides flexibility in studying behavior at large flow rates as the 3D printed material is rigid with Young's modulus 2870 MPa [40], in contrast to the elastomer PDMS (Young's modulus: 3 MPa [41]. The design allows integration of electrodes with an epoxy embedded PEEK nut; here we used Cu and Pt, but any other metals can be used, which is available in wire form. The design also allows easy cleaning of the wires with repolishing.

Cu electrodissolution was studied with the 3D printed cell to investigate current oscillations are large overpotientials close the limiting current region. Similar to PDMS results [19], subsequent LSV curves showed a decreasing limiting current, indicating that the recession of the electrode in the epoxy plays an important role in the response of the system. Nonetheless, current oscillation could be seen when an external resistance was attached to the electrode. The 3D printed setup has the practical advantage of long self-life after cleaning and the electrodes that are employed can be repolished and reused as desired. The PDMS flow channel shows deterioration and material damage after about 10 cell assemblies due to its more flexible nature. This could also increase reproducibility as newly prepared PDMS channels could have somewhat different flow channel sizes.

Finally, the 3D printed flow channel facilitated investigation of bistability and current oscillations for hydrogen oxidation. Built upon the results, 3D printing produces a gas impermeable microfluidic cell which can be used to study a variety of reactions such as hydrogen oxidation [26], carbon monoxide oxidation [42], and oxygen reduction [28] which are difficult to study in a standard PDMS flow cell. Moreover, the 3D printing also allows incorporation of multi-electrode arrays in the flow channels, using either separate PEEK nuts for large distance, or electrode arrays within a single nut for short distances, and these electrodes can be placed in 3D cells conveniently, which overcomes limitations of flow channel designs with PDMS based cells.

The results thus show 3D printed cells have the potential to provide a vehicle for studying nonlinear dynamics of electrochemical reactions for a wide range of cell geometries and electrode types and configurations. For example, oscillations with both *N*-NDR (copper electrodissolution) and HN-NDR type (hydrogen oxidation in the presence of inhibiting ions) were demonstrated. The cells in different configurations can be printed by CAD software design, which can enable investigations of cell/electrode geometry effects on nonlinear dynamics. In addition, recent progress in weakly nonlinear microfluidics [43] can enable coupling of complex chemical reaction with nonlinear fluidic effects.

## CRediT authorship contribution statement

**John A. Tetteh:** Investigation, Methodology, Formal analysis, Writing – review & editing. **Elizabeth A. Hayter:** Investigation, Software, Methodology. **R. Scott Martin:** Conceptualization, Methodology, Writing – review & editing. **István Z. Kiss:** Conceptualization, Methodology, Investigation, Formal analysis, Writing – original draft, Software.

## Declaration of Competing Interest

The authors declare that they have no known competing financial interests or personal relationships that could have appeared to influence the work reported in this paper.

## Acknowledgements

I.Z.K. acknowledges support from the National Science Foundation (NSF) under Grant No. CHE-1900011. The authors thank Major Selemani for help with constructing the Pt electrode.

## References

[1] J.L. Hudson, T.T. Tsotsis, Electochemical Reaction Dynamics: A Review, Chemical Engineering Science 49 (10) (1994) 1493.
[2] K. Krischer, Nonlinear Dynamics in Electrochemical Systems, Advances in Electrochemical Science and Engineering (2002) 89–208.
[3] M.T.M. Koper, P. Gaspard, The modeling of mixed-mode and chaotic oscillations in electrochemical systems, The Journal of Chemical Physics 96 (1992) 7797.
[4] Albahadily, F. N.; Schell, M., An Experimental Investigation of Periodic and Chaotic Electrochemical Oscillations in the Anodic Dissolution of Copper in Phosphoric Acid. *Journal of Chemical Physics* **1988**, *88* (7), 4312.
[5] I.Z. Kiss, V. Gáspár, L. Nyikos, Stability Analysis of the Oscillatory Electrodissolution of Copper with Impedance Spectroscopy, The Journal of Physical Chemistry 102 (6) (1998) 909–914.
[6] I.Z. Kiss, Z. Kazsu, V. Gáspár, Scaling relationship for oscillating electrochemical systems: dependence of phase diagram on electrode size and rotation rate, Physical Chemistry Chemical Physics 11 (35) (2009) 7669–7677.
[7] M. Urvölgyi, V. Gaspar, T. Nagy, I.Z. Kiss, Quantitative dynamical relationships for the effect of rotation rate on frequency and waveform of electrochemical oscillations, Chemical Engineering Science 83 (2012) 56–65.
[8] K. Krischer, H. Varela, Handbook of Fuel Cells. *Handbook of Fuel Cells - Fundamentals*, Technologies, and Applications 679 (2003).

[9] J. Vondrák, B. Klápště, J. Velická, M. Sedlaříková, R. Černý, Hydrogen–oxygen fuel cells, Journal of Solid State Electrochemistry 8 (1) (2003) 44–47.
[10] A.B. Stambouli, E. Traversa, Fuel cells, an alternative to standard sources of energy, Renewable and Sustainable Energy Reviews 6 (2002) 297–306.
[11] K. Krischer, M. Lubke, W. Wolf, M. Eiswirth, G. Ertl, Chaos and Interior Crisis in an Electrochemical Reaction, Berichte De Bunsen-Gesellschaft Fur Physikalsche Chemie 95 (7) (1991) 820–823.
[12] K. Krischer, M. Lubke, W. Wolf, M. Eiswirth, G. Ertl, Oscillatory Dynamics of the Electrochemical Oxidation of H2 in the Presence of Cu2+: Structure Sensitivity and the Role of Anions, Electrochimica Acta 40 (1) (1995) 69–81.
[13] H. Varela, K. Krischer, Nonlinear Phenomena during Electrochemical Oxidation of Hydrogen on Platinum Electrodes, Catalysis Today 70 (4) (2001) 411–425.
[14] C. Amatore, N.D. Mota, C. Sella, L. Thouin, Theory and experiments of transport at channel microband electrodes under laminar flows. 1. Steady-state regimes at a single electrode, Analytical Chemistry 79 (22) (2007) 8502–8510.
[15] R.S. Martin, P.D. Root, D.M. Spence, Microfluidic technologies as platforms for performing quantitative cellular analyses in an in vitro environment, The Analyst 131 (11) (2006) 1197–1206.
[16] A. Selimovic, A.S. Johnson, I.Z. Kiss, R.S. Martin, Use of epoxy-embedded electrodes to integrate electrochemical detection with microchip-based analysis systems, Electrophoresis 32 (8) (2011) 822–831.
[17] I.Z. Kiss, N. Munjal, R.S. Martin, Synchronized Current Oscillations of Formic Acid Electro-oxidation in a Microchip-based Dual-Electrode Flow Cell, Electrochimica Acta 55 (2) (2009) 395–403.
[18] J.C. McDonald, G.M. Whitesides, Poly(dimethylsiloxane) as a material for fabricating microfluidic devices, Accounts Chem Res 35 (7) (2002) 491–499.
[19] Y. Jia, A. Bi, A. Selimovic, R.S. Martin, I.Z. Kiss, Periodic and complex waveform current oscillations of copper electrodissolution in phosphoric acid in an epoxy-based microchip flow cell, Journal of Solid State Electrochemistry 19 (11) (2015) 3241–3251.
[20] A.G. Cioffi, R.S. Martin, I.Z. Kiss, Electrochemical Oscillations of Nickel Electrodissolution in an Epoxy-Based Microchip Flow Cell, Journal of Electroanalytical Chemistry 659 (1) (2011) 92–100.
[21] A. Birzu, Y. Jia, V. Sankuratri, Y. Liu, I.Z. Kiss, Spatially Distributed Current Oscillations with Electrochemical Reactions in Microfluidic Flow Cells, Chemphyschem : a European Journal of Chemical Physics and Physical Chemistry 16 (3) (2015) 555–566.
[22] Y. Jia, I.Z. Kiss, Decoding Network Structure in On-Chip Integrated Flow Cells with Synchronization of Electrochemical Oscillators, Scientific Reports 7 (2017) 46027.
[23] Y. Jia, I.Z. Kiss, Unidirectional Negative Coupling Induced Dynamical Patterns in an Epoxy-Based Dual-Electrode Microchip Flow Cell, Journal of the Electrochemical Society 165 (7) (2018) H374. H384.
[24] Y. Liu, I.Z. Kiss, Localization of current oscillations and synchronization patterns in microchip-based dual electrode flow cell without resistance balancing, Eur. Phys. J. Spec. Top. 227 (18) (2019) 2659–2673.
[25] T. Gervais, J. El-Ali, A. Günther, K.F. Jensen, Flow-induced deformation of shallow microfluidic channels, Lab on a Chip 6 (4) (2006) 500.
[26] D.A. Crespo-Yapur, A. Bonnefont, R. Schuster, K. Krischer, E.R. Savinova, Cooperative behaviour of Pt microelectrodes during CO bulk electrooxidation, Chemphyschem : a European Journal of Chemical Physics and Physical Chemistry 14 (6) (2013) 1117–1121.
[27] S.M. Mitrovski, L.C.C. Elliott, R.G. Nuzzo, Microfluidic Devices for Energy Conversion: Planar Integration and Performance of a Passive, Fully Immersed H2–O2 Fuel Cell, Langmuir 20 (17) (2004).
[28] S.M. Mitrovski, R.G. Nuzzo, An electrochemically driven poly(dimethylsiloxane) microfluidic actuator: oxygen sensing and programmable flows and pH gradients, Lab on a Chip 5 (6) (2005) 634–645.
[29] A.K. Au, W. Huynh, L.F. Horowitz, A. Folch, 3D-Printed Microfluidics, Angewandte Chemie, International Edition 55 (12) (2016) 3862–3881.
[30] A.V. Nielsen, M.J. Beauchamp, G.P. Nordin, A.T. Woolley, 3D Printed Microfluidics, Annual Rev. Anal. Chem. 13 (1) (2020) 45–65.
[31] J.L. Erkal, A. Selimovic, B.C. Gross, S.Y. Lockwood, E.L. Walton, S. McNamara, R. S. Martin, D.M. Spence, 3D printed microfluidic devices with integrated versatile and reusable electrodes, Lab on a Chip 14 (12) (2014) 2023–2032.
[32] A.S. Munshi, R.S. Martin, Microchip-based electrochemical detection using a 3-D printed wall-jet electrode device, The Analyst 141 (3) (2016) 862–869.
[33] I.C. Samper, S.A.N. Gowers, M.L. Rogers, D.-S.-R.-K. Murray, S.L. Jewell, C. Pahl, A. J. Strong, M.G. Boutelle, 3D printed microfluidic device for online detection of neurochemical changes with high temporal resolution in human brain microdialysate, Lab on a Chip 19 (11) (2019) 2038–2048.
[34] E.A. Hayter, S. Azibere, L.A. Skrajewski, L.D. Soule, D.M. Spence, R.S. Martin, A 3D-printed, multi-modal microfluidic device for measuring nitric oxide and ATP release from flowing red blood cells, Analytical Methods 14 (33) (2022) 3171–3179.
[35] E.A. Hayter, A.D. Castiaux, R.S. Martin, 3D-printed microfluidic device with in-line amperometric detection that also enables multi-modal detection, Analytical Methods 12 (15) (2020) 2046–2051.
[36] V.G. Levich, Physicochemical hydrodynamics, Prentice-Hall, Engelwood Cliffs, 1962.
[37] Y. Jia, I.Z. Kiss, Spontaneously Synchronized Electrochemical Micro-oscillators with Nickel Electrodissolution, The Journal of Physical Chemistry C 116 (36) (2012) 19290–19299.
[38] M. Eiswrith, M. Lubke, K. Krischer, W. Wolf, J.L. Hudson, G. Ertl, Structural Effects on the Dynamics of an Electrocatalytic Oscillator, Chemical Physics Letters 192 (2–3) (1992) 254–258.
[39] K. Krischer, M. Lubke, M. Eiswirth, W. Wolf, J.L. Hudson, G. Ertl, A Hierarchy of Transitions to Mixed Mode Oscillations in an Electrochemical System, Physica D: Nonlinear Phenomena 62 (1–4) (1993) 123–133.
[40] P. Zmarzły, D. Gogolewski, T. Kozior, Design guidelines for plastic casting using 3D printing, Journal of Engineered Fibers and Fabrics 15 (2020) 1–10.
[41] I.D. Johnston, D.K. McCluskey, C.K.L. Tan, M.C. Tracey, Mechanical characterization of bulk Sylgard 184 for microfluidics and microengineering, Journal of Micromechanics and Microengineering 24 (3) (2014) 035017.
[42] D.J. Case, Y. Liu, I.Z. Kiss, J.-R. Angilella, A.E. Motter, Braess's paradox and programmable behaviour in microfluidic networks, Nature 574 (7780) (2019) 647–652.
[43] D. Stoecklein, D. Di Carlo, Nonlinear Microfluidics, Analytical Chemistry 91 (1) (2019) 296–314.